A novel approach to the analysis of distributed shear banding in polymer blends

Pijnenburg, KGW; Van der Giessen, E

Published in:
International Journal for Numerical Methods in Engineering

DOI:
10.1002/nme.792

INTERNATIONAL JOURNAL FOR NUMERICAL METHODS IN ENGINEERING
Int. J. Numer. Meth. Engng 2003; **58**:703–721 (DOI: 10.1002/nme.792)

A novel approach to the analysis of distributed shear banding in polymer blends

K. G. W. Pijnenburg[1] and E. Van der Giessen[1,2,*,†]

[1]*Delft University of Technology, Koiter Institute, Mekelweg 2, 2628 CD Delft, The Netherlands*
[2]*Department of Applied Physics, University of Groningen, Nijenborgh 4, 9747 AG Groningen, The Netherlands*

SUMMARY

The toughness of glassy polymers can be enhanced by blending with rubber particles. The consensus is that this toughening is due to massive plastic deformation of the matrix that takes place once the particles have cavitated. Micromechanical studies of regular stackings of particles in a polymer matrix have provided much insight into the localized plastic flow in blends at the microscale of individual particles (or voids, once cavitated). Even some steps towards macroscopic constitutive models have been made. However, at intermediate length scales (i.e. larger than several particles, but smaller than the scale at which the material may be regarded as homogeneous) the situation is unclear. It is this length scale that becomes important around crack tips, for example, where a thorough understanding of the toughening effect has to be derived from. In this paper, we therefore present a novel approach to the analysis of distributed shear banding in polymer–rubber blends. A coarse-grain description, in which much of the morphology is retained but the local shear banding is idealized into 'shear surfaces', will enable us to analyse ensembles with large numbers of particles. The parameters of this model will be validated with results from detailed cell analyses. Copyright © 2003 John Wiley & Sons, Ltd.

KEY WORDS: plasticity; polymers; finite elements; cohesive surfaces; shear bands

1. INTRODUCTION

It seems fair to state that homogenization approaches for linear materials are well developed by now. Work is underway for non-linear materials but this faces many technical difficulties. Once these homogenization methods are available, it is expected from experience with e.g. linear composites that they will find widespread application to relate the overall deformation behaviour of non-linear composites to that of the constituents. Their relevance for

*Correspondence to: E. Van der Giessen, Department of Applied Physics, University of Groningen, Nijenborgh 4, 9747 AG Groningen, The Netherlands.
†E-mail: e.van.der.giessen@phys.rug.nl

Received 21 May 2001
Revised 6 November 2002
Accepted 6 November 2002

fracture of the same materials is, at least, limited—after all, fracture is about localization and not about homogenization.

We think that this is particularly true for material systems in which the constituents themselves have a strong tendency for strain localization. Important examples of such systems are so-called polymer blends. Blends are 'composites' in which around 30% volume of micron-scale rubber particles are mixed in a cheap matrix, with the prime purpose of increasing the fracture toughness of the material. Recent years have shown a growing consensus regarding the mechanisms responsible for this toughening [1]. Experimental evidence suggests that cavitation of the rubber particles and the associated reduction in triaxial stress states, leads to large plastic zones in the polymer matrix. The accompanied dissipation of energy gives blends their enhanced toughness. Without the relief of triaxiality due to cavitation, crazes would be formed, leading to brittle fracture. Cavitation is excluded in sufficiently stiff particles and blends with these kinds of particles do not exhibit toughening [1, 2]. We confine attention here to blends with low-modulus rubber particles which do exhibit rubber cavitation.

Material models for both glassy polymers and rubbers have been known for quite some time now [3]. The problem in describing blends lies therefore not in the material behaviour of the constituents, but in the difference between the size of the plastic zone (the 'meso' scale) and the smaller size scale of the rubber particles at which the competition between crazing and plastic deformation takes place (the 'micro' scale). Several researchers have therefore simplified the problem by looking at regular stackings of voids (cavitated rubber particles) in a polymer matrix, thereby making the plastic zone in effect infinitely large. Detailed finite element computations of the deformation processes around one or two voids have been carried out under different remote loading conditions (e.g. References [4–8]). Cells with larger numbers of voids have recently been analysed in two dimensions (2D) but with somewhat less detail [9].

Partly motivated by such studies, some efforts have been taken during recent years in establishing macroscopic constitutive models for cavitated amorphous polymers, e.g. References [4, 10, 11]. In such models the rubber particles, once cavitated, are replaced with voids since the rubber modulus is in practice much smaller than that of the matrix. There is a potential limitation of such macroscopic, homogenized models to describe the state around a crack tip, which is critical to understand the toughening effect. The basic reason is that such a macroscopic constitutive model, by definition, describes the overall response of a sample of the blend which is so large that it contains sufficiently many particles for it to be statistically meaningful. At the same time, the sample size should be smaller than the characteristic wavelength of the fields near the crack tip. This may be a conflict. The solution to this may be a coarse-grained model of the microstructure, which is capable of describing many particles, while retaining the relevant details of the plastic deformation in between the particles.

The detailed 2D cell studies mentioned above [4–7, 11] have shown that the plastic deformation around individual cavitated particles takes place in narrow shear bands in between two particles. This observation is the starting point for the coarse-grained model we introduce in this paper. Instead of modeling every particle in detail to capture all features of the shearing process, we propose to represent the shear bands in an idealized manner by surfaces that can slide over one another. We validate the model by comparing it to detailed cell analyses.

2. SHEAR SURFACE FORMULATION

2.1. The concept of a shear surface

Detailed 2D finite element studies (e.g. References [4, 5, 7, 11]) have shown that plastic flow in the matrix between the cavitated particles (often treated as voids, as done in the sequel) occurs by shear bands that evolve in size and shape with the overall deformation. This is an immediate consequence of the typical strain softening after yield and the subsequent orientation hardening (see inset in Figure 1(a)). It has also been observed [6] that at the critical moment of overall yield and strain softening, the shear bands typically connect neighbouring voids, lying in or close to the shearing direction. Figure 1(a) gives an example of this, showing the typical shear band structure in a doubly periodic array of single-void cells under remote shear. The shear band is visualized in terms of the distribution of the current plastic shear strain rate (denoted by $\dot{\gamma}^{\mathrm{p}}$) compared to the applied shear rate $\dot{\bar{\gamma}}$. Outside the intense shear band, the material responds essentially elastically.

When making the scale transition from this micro-scale to the meso-scale of a blend comprising of many particles, we cannot and do not want to retain the fine details of the shear banding. Therefore, the idea is to idealize the shear band in Figure 1(a) by just a surface, with the shearing in the shear band collapsed into the relative 'sliding' of the two surfaces, as shown in Figure 2. the response of the material inside the actual shear band is then transferred into a relation between the shear traction τ versus the relative shear displacement Δ_t in such a way that the average material behaviour (Figure 1(b)) is the same. When such potential shear surfaces are introduced between all nearest-neighbour particles in the blend, a triangulation results as shown in Figure 3 for 500 randomly distributed voids of the same size. The triangles bounded by shear surfaces are interpreted as triangular finite elements (see also Figure 2(a)). They describe the bulk elastic behaviour in an approximate sense, with a similar type of resolution as for the localized shearing. Owing to this construction, the particle/void microstructure determines the finite element mesh and the shear surfaces. For a given configuration of voids, there is some ambiguity in how to place shear surfaces in between particles. We have chosen to use Delaunay triangulation, and this gives a unique mesh.

Figure 2(b) shows a shear surface in detail. Its main characteristics are the direction $\mathbf{t}$, the unit normal $\mathbf{n}$ and the length l of the ligament between the two adjacent voids with radius r_{v}. Initially, the node pairs $(1,3)$ and $(2,4)$ coincide with the two respective void centres. The degrees of freedom of the shear surface are the relative displacements $\mathbf{\Delta}_i$ $(i=1,2)$ of these node pairs. The components Δ_n and Δ_t in $\mathbf{n}$ and $\mathbf{t}$-direction, respectively, give the normal opening and tangential sliding of the two faces with respect to each other. The conjugate tractions σ and τ in normal and tangential direction, respectively, should follow from integration of a suitable constitutive equation along the ligament. This closely follows the idea of cohesive surfaces embedded between finite elements as pioneered by Xu and Needleman [12]. The difference is that cohesive surfaces are used to simulate fracture and are governed predominantly by their normal response [12, 13], whereas the shear surfaces introduced here are designed to pick up localized shearing. This is all governed by the shear surface constitutive law to be discussed subsequently.

2.2. Constitutive equations for a shear surface

The constitutive equation for a shear surface is to be constructed so that it provides an approximation of the response of a shear band between voids as predicted by full detail

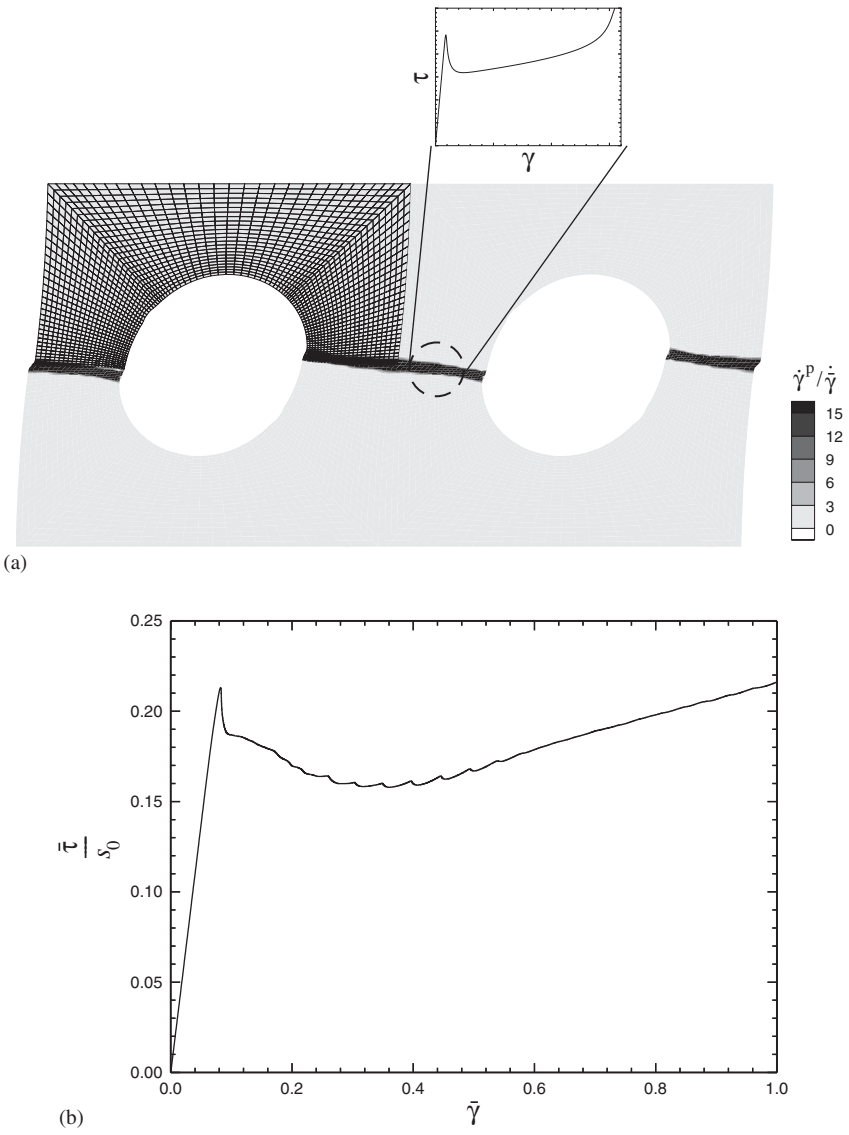

Figure 1. (a) Micro-scale distribution of plastic shear rate $\dot{\gamma}^p$ (normalized by the applied overall shear rate $\dot{\bar{\gamma}} = 10^{-2}\,s^{-1}$) in between voids (cavitated particles) subjected to remote simple shear [6]. The inset shows the shear stress τ vs shear strain γ response of the matrix material; and (b) mesoscopic response of the blend model of (a), in terms of overall shear stress $\bar{\tau}$ versus shear strain $\bar{\gamma}$.

(2D) finite element studies. The material description in these kind of studies (see References [4–6] for details) features elastic-viscoplasticity, with softening immediately after yield and re-hardening at large strains. We use these continuum constitutive relations to motivate the constitutive equation for a shear surface. Obviously, the material parameters can be

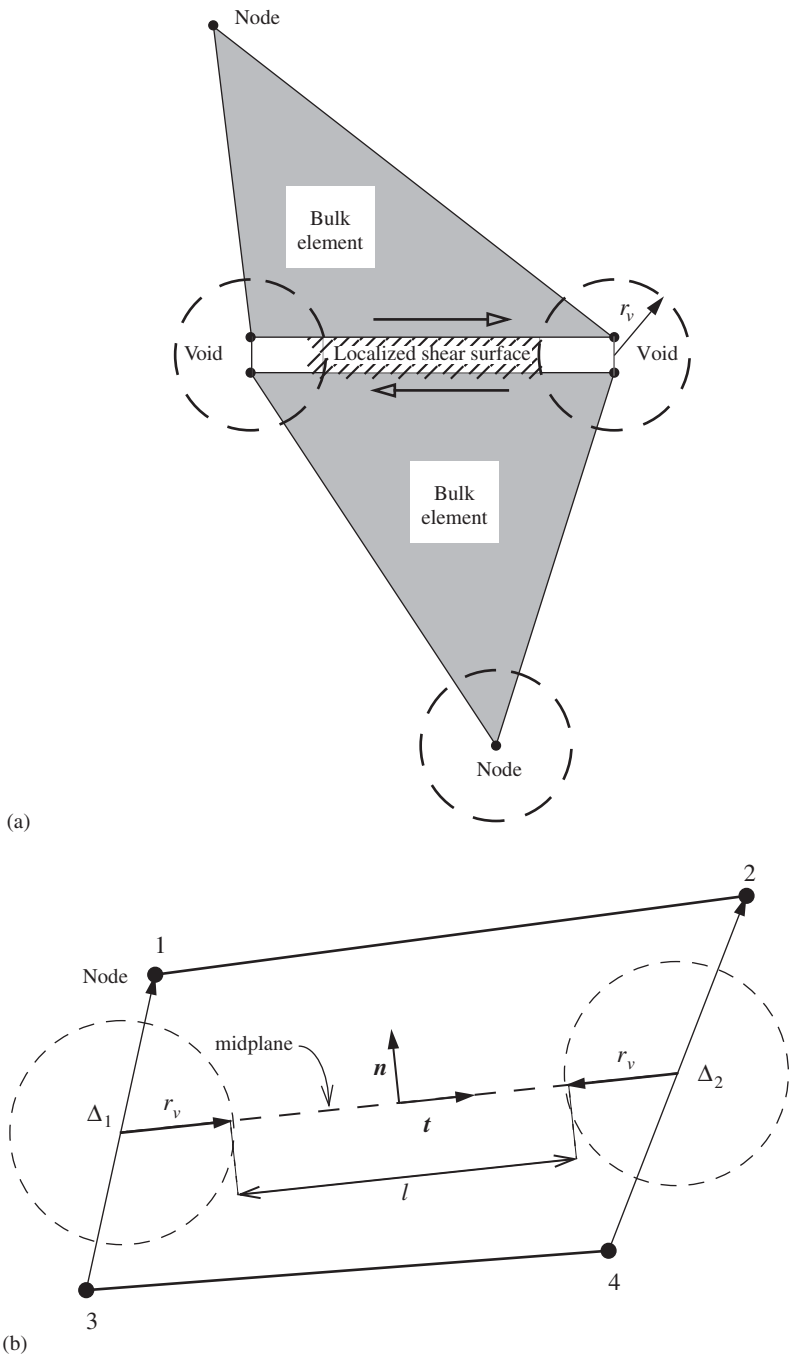

Figure 2. (a) Idealization of localized shearing in a 'shear surface', connecting two triangular bulk elements; and (b) detailed view of a shear surface.

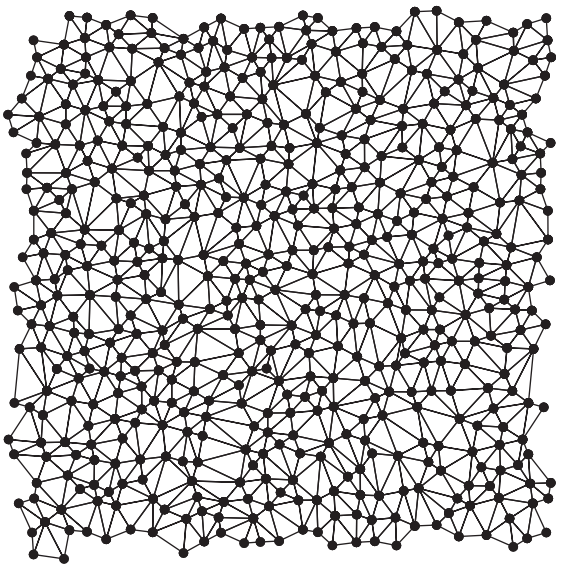

Figure 3. Random arrangement of 500 rubber particles/voids in a periodic cell of a glassy matrix in two dimensions. The lines connecting neighbouring particles define 'shear surfaces', with the triangles being used as triangular bulk elements.

quite different (the shear surface parameters are distinguished by a subscript s), because they now have to represent the overall behaviour in a shear band.

In analogy with the continuum formulation, we split the shear displacement Δ_t into an elastic, Δ_t^{e}, and a plastic part, Δ_t^{p}. For the elastic part, we write

$$\dot{\tau} = \frac{\zeta}{r_{\mathrm{v}}} G\dot{\Delta}_t^{\mathrm{e}} = \frac{\zeta}{r_{\mathrm{v}}} G(\dot{\Delta}_t - \dot{\Delta}_t^{\mathrm{p}}) \tag{1}$$

where a superposed dot signifies the time derivative and G is the shear modulus of the bulk. The dimensionless coefficient ζ serves as a fitting factor to keep the elastic shear displacements low. The reason for this is that the introduction of shear surfaces in between all bulk elements increases the overall compliance of the blend (the analogous effect of embedded cohesive zones is well known, see e.g. References [12, 13]). The additional compliance needs to be small, but the stiffness of the shear surfaces should not be so large that it compromises the condition of the final, overall stiffness matrix. Introduction of the void radius r_{v} in (1) ensures that the dimensions are correct. Furthermore it introduces the correct scaling with sample size. This last requirement can be made more clear as follows. Consider a sample subjected to an applied shear rate. Doubling all linear dimensions will also double the displacements (like Δ_t^{e}) and would, without compensation, give a twice as high $\dot{\tau}$. Such dependence on sample size is obviously not allowed and is corrected for by normalization with r_{v}.

The plastic part of the shear velocity $\dot{\Delta}_t^{\mathrm{p}}$ is expressed in the form

$$\dot{\Delta}_t^{\mathrm{p}} = \beta r_{\mathrm{v}} \dot{\gamma}^{\mathrm{p}} \tag{2}$$

where $\dot{\gamma}^{\mathrm{p}}$ is a plastic shear strain rate. Here again we have the void radius r_{v} for dimensional consistency. The coefficient β will serve to adjust the stress value at which plastic flow starts. The main reason for writing (2) is that we can now employ the same constitutive expression, due to Argon [14], as used in the fine-scale continuum viscoplasticity model adopted for Figure 1:

$$\dot{\gamma}^{\mathrm{p}} = \dot{\gamma}_0 \exp\left[-\frac{As}{T}\left\{1-\left(\frac{\tau-\tau_{\mathrm{h}}}{s}\right)^{5/6}\right\}\right] \tag{3}$$

with $\dot{\gamma}_0$ being a reference strain rate, T being temperature and A a material constant. Here, s is the athermal shear strength, which is taken to evolve from its initial value s_0 to a steady state value s_{ss} according to

$$\dot{s} = h_{\mathrm{s}}(1 - s/s_{\mathrm{ss}})\dot{\gamma}^{\mathrm{p}} \tag{4}$$

Pressure (p) sensitivity of yield is accounted for by replacing s in (3) by $s + \alpha_{\mathrm{s}} p$ with α_{s} a pressure-sensitivity parameter. The value of α_{s} is expected to be different from that in the continuum formulation, since some detail of the local pressure variations around the voids is lost in the shear surface model.

The back stress τ_{h} in (3) describes the hardening taking place inside the shear band due to the stretching of the molecules. In the continuum constitutive model, the three-dimensional hardening law is based on considerations of the molecular processes (see, e.g. References [3, 15]) and gives rise to linear strain hardening initially, followed by highly non-linear hardening. The hardening relation we propose in the shear surface model is instead taken as a simple linear function of the shear displacement in the shear surface, i.e.

$$\tau_{\mathrm{h}} = C_{\mathrm{s}}^{\mathrm{R}} \Delta_t \tag{5}$$

with $C_{\mathrm{s}}^{\mathrm{R}}$ the hardening modulus. This is justified by the observation (e.g. Reference [4]) that the process of shear band propagation in the ligament in between the voids smears out the local, non-linear hardening to a more gradual one.

The constitutive response of a shear surface is shown schematically in Figure 4, including the meaning of the material parameters. This response is reminiscent of that of the underlying bulk amorphous polymer under shear, but the values of the material parameters should be expected to be different. Although plasticity is actually confined to highly localized shear bands in the ligament between voids, it is unrealistic to expect that the same parameters that govern plastic flow in the detailed continuum model will be valid for the idealized shear surfaces without any adjustments. In particular, besides ζ and β, which control the overall elastic modulus and the yield point, we consider h_{s}, α_{s} and $C_{\mathrm{s}}^{\mathrm{R}}$ as tunable parameters, which we will fit to detailed analyses in the next section.

Since we are only interested in shearing of the surface, we want the normal opening to be negligible. The easiest way to enforce that is by giving the shear surface a high stiffness against normal displacements, i.e.

$$\sigma = \frac{c}{r_{\mathrm{v}}} E \dot{\Delta}_n \tag{6}$$

where E is the Young's modulus of the matrix and c is an adjustable multiplication factor. As before, r_{v} is included for appropriate scaling. The value taken for c is 100; this is high

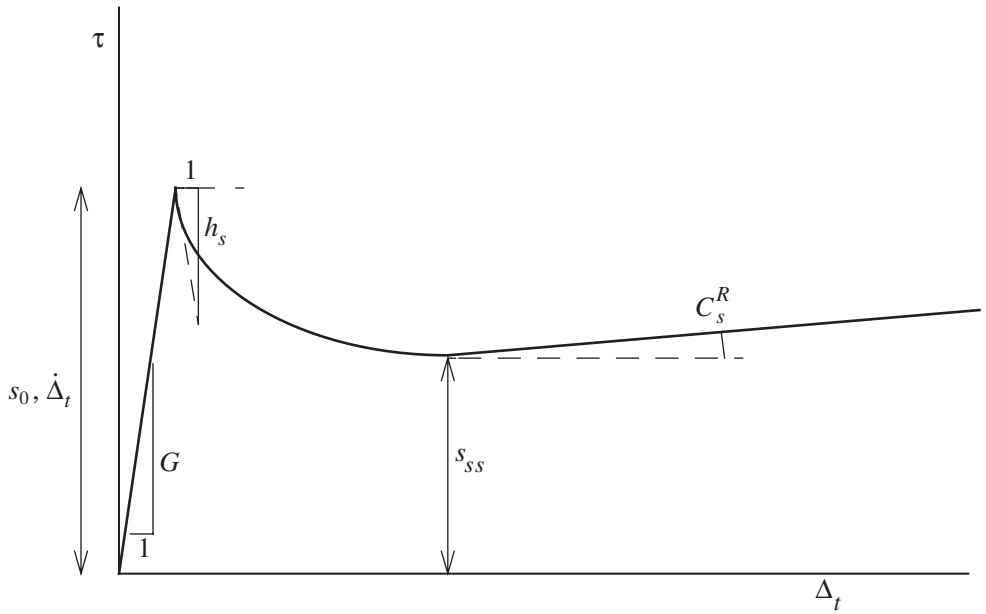

Figure 4. Schematic view of the constitutive response of a shear surface for amorphous polymers and its material parameters.

enough to keep the normal opening sufficiently small and low enough not to cause numerical problems.

2.3. Numerical implementation

The formulation in the previous subsection allows the concept of a shear surface to be implemented in any finite element code as an interface element. Application to a blend, as discussed in Section 2.1, requires that all continuum elements are interconnected by such surface elements, but this is completely similar to the use of embedded cohesive surfaces in References [12, 13]. One point worth mentioning is that the contribution of each shear surface to the total virtual work is evaluated by numerical integration over the ligament length l between voids (see Figure 2). We use two integration points located at $\pm\sqrt{3}l/6$ from the centre of the ligament.

It is also worthwhile to note that the expression (3) for the plastic shear velocity $\dot{\Delta}_t^{\mathrm{p}}$ is highly non-linear. A forward gradient formulation, similar to that for the continuum formulation [16] can therefore greatly enhance the numerical stability of the calculations and thereby increase the stable time-step size. This is done by making an estimate of the average $\dot{\Delta}_t^{\mathrm{p}}$ during the current time step Δt of the form $\dot{\Delta}_t^{\mathrm{p}} = (1-\theta)\dot{\Delta}_t^{\mathrm{p}}(t) + \theta\dot{\Delta}_t^{\mathrm{p}}(t+\Delta t)$ with $\theta \in [0,1]$. The latter term can be estimated through a series expansion of (2)–(3) in terms of τ. After elimination of $\dot{\tau}$ from this expansion by means of the elasticity law (1), we obtain

$$\dot{\Delta}_t^{\mathrm{p}} = \frac{\dot{\Delta}_t^{\mathrm{p}}(t) + \chi\dot{\Delta}_t(t)}{1+\chi} \tag{7}$$

with

$$\chi = \theta \Delta t \, \frac{\partial \dot{\Delta}_t^{\mathrm{p}}}{\partial \tau} \, \frac{\zeta}{r_{\mathrm{v}}} \, G \tag{8}$$

When (7), along with $\dot{\Delta}_t^{\mathrm{p}}(t)$ from (2)–(3) on the basis of all quantities evaluated at time t, is used in (1), this gives rise to a rate tangent modulus that depends on the current time step.

3. VALIDATION

Using a simple doubly periodic array of voids as shown in Figure 5 we can directly compare the shear surface model to the detailed cell calculations performed previously [6, 11]. The morphology being identical, the shear surface model involves only two elastic, bulk finite elements and five cohesive surface elements. First, the material parameters in the shear surface model will be fitted for a case where the void array is square, $a = b$ in Figure 5, and the void volume fraction is 20%. Computations with different void volume fractions and different aspect ratios b/a of the cell will be used in Section 3.2 to verify the model. In each case the loading is applied through prescribed horizontal (and zero vertical) displacements at the top and bottom, resulting in overall simple shear at a rate of $\dot{\bar{\gamma}} = \sqrt{2} \times 10^{-2}\,\mathrm{s}^{-1}$. Periodic boundary conditions are prescribed along the left and right-hand sides of the cell.

3.1. Material parameter selection

It bears emphasis that the constitutive model used in the detailed computations is completely similar in spirit to that formulated in Section 2.2. Referring to [6, 11] for details

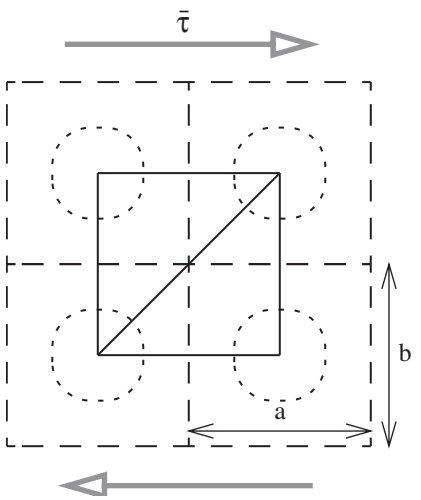

Figure 5. Configuration used to fit the parameters in the constitutive model for the shear surface. Dashed lines show four unit cells in a doubly periodic array of voids. One of these cells is analyzed in detail with a mesh of the type shown in Figure 1. The solid lines show the two-element mesh used in the shear surface calculations. There are shear surfaces along all sides of the elements.

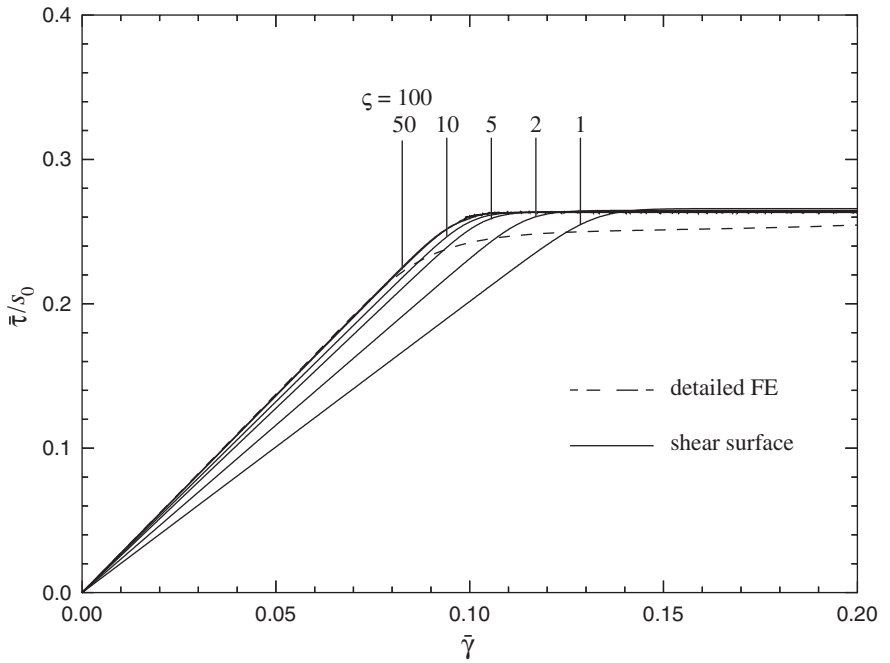

Figure 6. The influence of the parameter ζ on the initial elastic slope of the stress–strain curve in the shear surface model (Figure 5, $b/a = 1$).

of this model, it suffices to report here the material parameters (typically for SAN) used: Young's modulus $E = 1500$ MPa; Poisson's ratio $v = 0.38$; $s_0 = 119.5$ MPa; $s_{ss} = 95.0$ MPa; $\dot{\gamma}_0 = 1.06 \times 10^8$ s^{-1}; $A = 129.2$ K; $T = 296$ K; $\alpha = 0.25$; $h = 1500$ MPa; $C_s^R = 4.0$ MPa. The values of those parameters that also emerge in the shear surface model, i.e. $G = E/2(1 + v)$, s_0, s_{ss} and $\dot{\gamma}_0$, are directly copied. The softening and hardening parameters in the shear surface model, h_s and C_s^R, are different from h and C^R and are to be fitted. In addition, we will determine the value of ζ, β and α_s in order to give a best match of the overall stress–strain curves predicted by the two models. The strategy in fitting the parameters is that we will first focus on the elastic response, than the yield point, etc. In doing so, we may temporarily put certain material parameters to zero in order not to mix effects.

Since the voids are not represented explicitly in the shear surface model, the effect of porosity should be incorporated in the elastic constants of the bulk elements directly. In an isotropic material only two constants would be needed, and these can be readily estimated from the matrix properties and the void volume fraction using well-known micromechanics expressions (see, e.g., Reference [11]). Our model material is essentially anisotropic and under general loading conditions, would therefore need more than two constants. However, since we will only be looking at one type of (shear) loading, it is possible to characterize the elastic behaviour using only an effective value of Poisson's ratio v and Young's modulus E. The values we have used are $v = 0.38$ and $E = 900$ MPa, as found from the elastic response found in the cell calculations for a blend containing a void volume fraction of 20%.

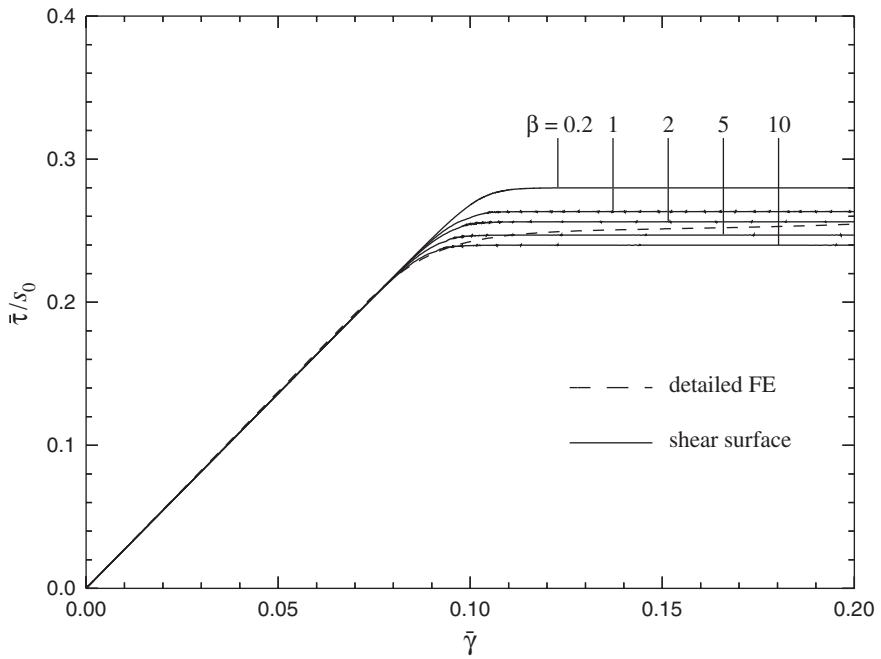

Figure 7. The influence of the parameter β on the overall yield stress of the shear surface model (Figure 5, $b/a = 1$), without softening and hardening, and without pressure sensitivity.

We start with determining the value of ζ, which governs the elastic response of the shear surfaces. As discussed above, the value of ζ should be made as large as possible in order to minimize the extra overall compliance, but not so large to cause numerical problems. Figure 6 shows the dependence of the elastic slope on ζ. It is seen that for low values of ζ the elastic response indeed is too soft compared to the detailed cell results. A value of $\zeta = 50$ is high enough to keep the difference in elastic response smaller than 1%.

The parameter β in (2) controls the amount of plastic displacement in the shear surface, and therefore the instant at which yielding takes place (characterized by $\dot{t} = 0$ or $\dot{\Delta}_t = \dot{\Delta}_t^{\mathrm{p}}$). A large value for β results in early and much plasticity, corresponding to a low yield stress. Figure 7 shows the material response for various values of β. It should be noted that in both the detailed and the shear surface calculations we have switched off softening and hardening, i.e. put $h = C^{\mathrm{R}} = 0$ and $h_{\mathrm{s}} = C_{\mathrm{s}}^{\mathrm{R}} = 0$, as well as pressure sensitivity, $\alpha = 0$ and $\alpha_{\mathrm{s}} = 0$. We conclude from Figure 7 that $\beta = 2$ gives a good agreement.

Before we introduce softening, we have to include the pressure dependence of plastic flow (see Equation (4) and accompanying text) first. This might seem odd, since we are considering shear, which does not have a hydrostatic component in homogeneous materials. However, as soon as plasticity starts the material is no longer homogeneous and pressure effects will become noticeable. Before we can go to the large (plastic) strains that go with softening and hardening we therefore have to include the pressure dependence. We cannot assess the value of the parameter α_{s} from shear calculations up to yield alone, as the hydrostatic stress

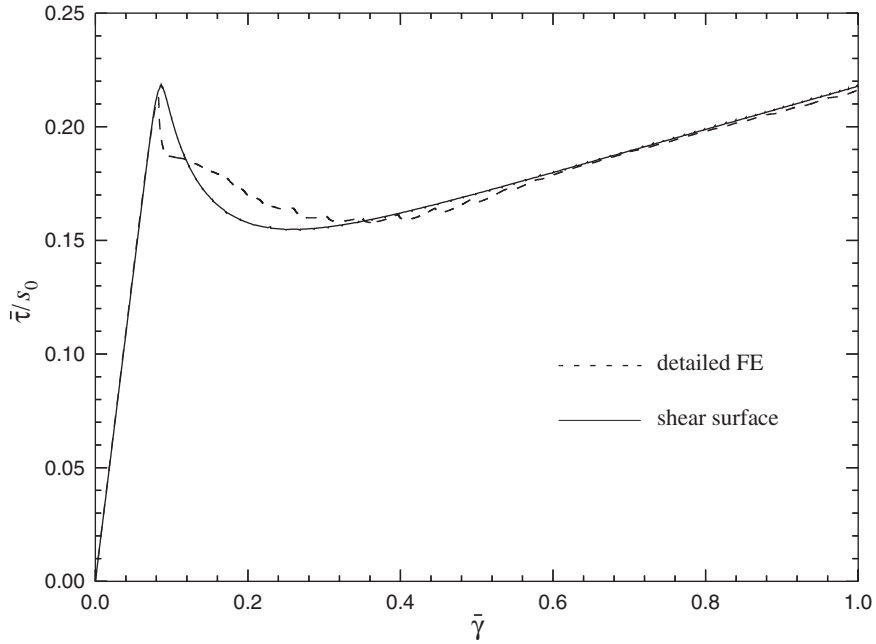

Figure 8. Overall stress–strain curve of the shear surface model (Figure 5, $b/a = 1$) after fitting of all parameters (see text), compared with that of detailed cell calculations.

is still small at that stage. Therefore we superimpose some hydrostatic stress to the shear deformation. This is done by adding a small vertical and horizontal strain rate to the applied loading (see Figure 5). At the moment of yield (i.e. when $\dot{\tau} = 0$) we know the applied stress $\bar{\boldsymbol{\sigma}}$, from which we find the overall hydrostatic stress

$$\Sigma_{\mathrm{m}} = \tfrac{1}{3} \operatorname{tr} \bar{\boldsymbol{\sigma}} \tag{9}$$

and the Von Mises equivalent stress

$$\Sigma_{\mathrm{e}} = \sqrt{\tfrac{3}{2} (\bar{\boldsymbol{\sigma}} - \tfrac{1}{3} \operatorname{tr} \bar{\boldsymbol{\sigma}}) : (\bar{\boldsymbol{\sigma}} - \tfrac{1}{3} \operatorname{tr} \bar{\boldsymbol{\sigma}})} \tag{10}$$

With these values, we can construct part of the yield surface in Σ_{e}–Σ_{m} space, thus emphasizing the pressure dependence of yield. By comparing the detailed cell results to those of the shear surface model for various values of additional hydrostatic stress and different α_{s} it is possible to find the value of α_{s} that gives the best agreement.

A drawback of this procedure is that the yield point is not easily found in the curves (see Figure 7), since the stationary τ value is approached almost asymptotically for the present material parameters. In order to get a more pronounced (and more realistic) peak, we already introduce some softening into the model, although we do not yet know what value the softening parameter h_{s} in the shear surface model should have. Introducing a non-zero h_{s} mainly affects the post-yield behaviour and has only a minor influence on the yield stress itself. Moreover, the effect on the yield point is the same for a wide range of values for h_{s}.

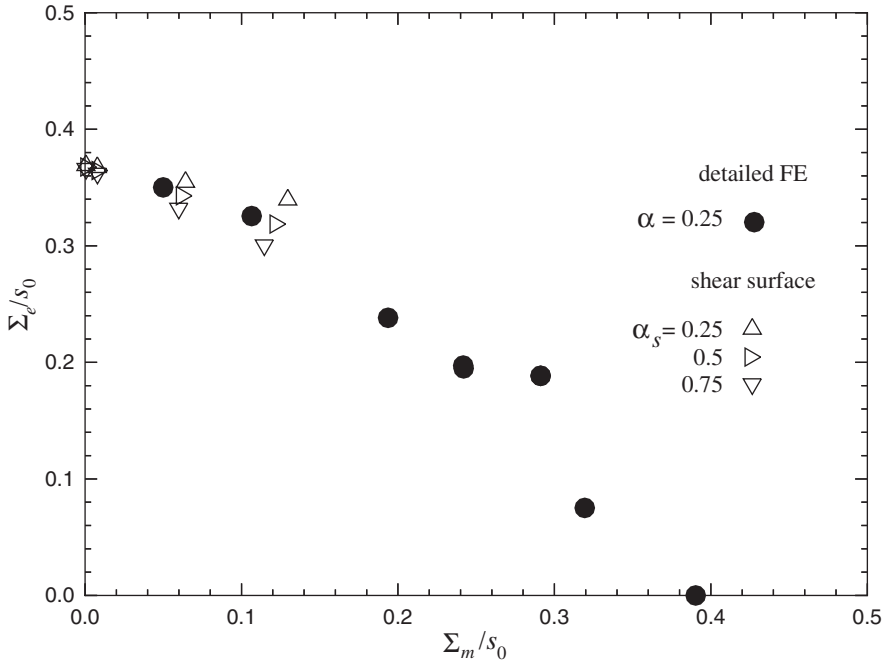

Figure 9. Pressure dependence of the overall yield point in the shear surface model (Figure 5, $b/a = 1$), for various values of α_s.

Since softening needs to be included anyway, we can immediately compensate for this by adjusting β in (2) to the new yield stress. It is found that $\beta = 50$ gives good agreement in this situation, as opposed to $\beta = 2$ that was found in Figure 7 for the case of perfect plasticity. Now, taking any value of h_s (we took $h_s = 5000$ MPa) that gives a distinct yield point, for the moment, serves our purpose of determining the pressure dependence coefficient α_s. The yield points in Σ_e–Σ_m space obtained in this way (not shown) reveal that $\alpha_s = 0.5$ gives good agreement with the detailed cell calculations.

Unfortunately, the last two characteristics, softening and hardening, cannot be conveniently separated, since changing the softening affects the hardening response and vice versa. Because of this, it is not possible to make separate plots of a series of h_s or C_s^R values showing the convergence to the detailed cell results. However, an iterative procedure enables to find a set of parameters that reproduces the overall post-yield behaviour of the blend adequately. We find that $h_s = 15000$ MPa and $C_s^R = 125$ MPa give good overall results, as shown in Figure 8. As a final check, to be sure that the value of α_s is indeed correct when softening and hardening are included, we have repeated the procedure for determining α_s, this time including all newly found parameters in the calculations. These are the results shown in Figure 9. It is seen that also in this case $\alpha_s = 0.5$ is an appropriate value.

3.2. Verification

All calculations so far have been done for one particular void volume fraction of 20%, and for a square void array. To validate our parameters, we have also performed calculations

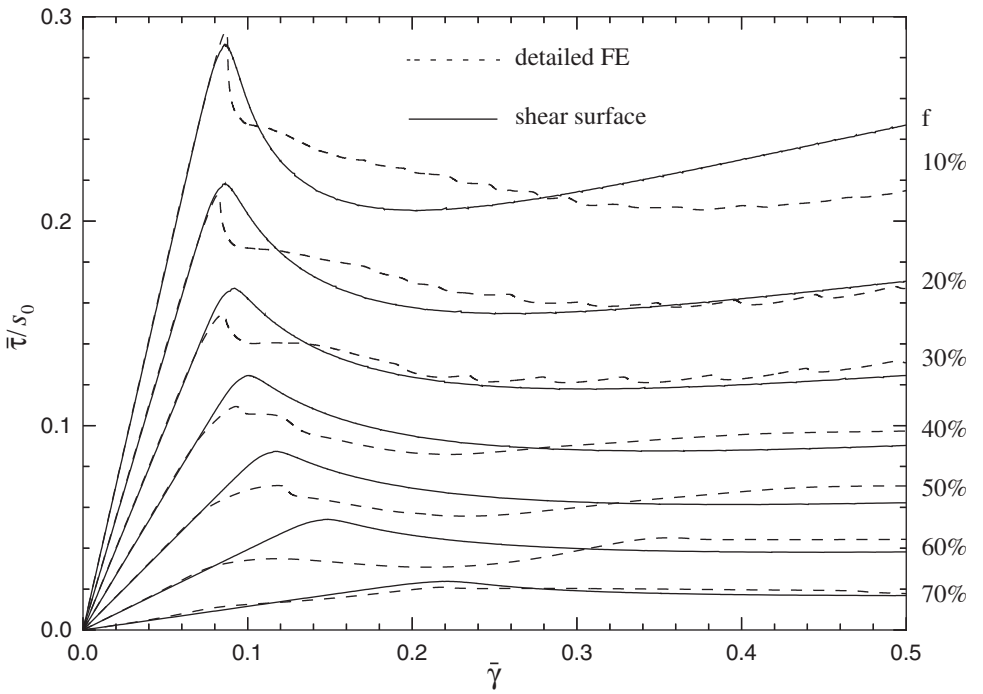

Figure 10. Comparison of stress–strain curves of the shear surface model (Figure 5, $b/a = 1$) with the cell calculations for different void volume fractions.

with different void volume fractions and different morphologies. These results, keeping all material parameters in the shear surface model the same as before, are summarized in Figures 10 and 11. Figure 10 shows that for a wide range of volume fractions and void configurations we get quite satisfactory agreement with detailed cell calculations. Although the general behaviour is captured quite well, two remarks should be made. First, the yield point predicted by the shear surface model tends to overestimate that of the cell results when the void volume fraction increases. Second, the hardening for a volume fraction of 10% appears to be too strong; it should be noted however that this is the low end of rubber volume fraction in real blends.

Another way to change the morphology of the blend is to vary the stacking of the voids, i.e. to change the aspect ratio b/a of the basic cell of Figure 5. Going from a square array of voids to a rectangular stacking in Figure 11, we find that these morphologies are still well described by the same parameters. We may therefore conclude that the parameters as we have determined them really apply to the blend itself and not just to a particular representation.

4. PREDICTION

Now that the shear surface model has been tested and verified for regular stackings of the voids, we consider a problem that exemplifies the power of the method. As an example, we

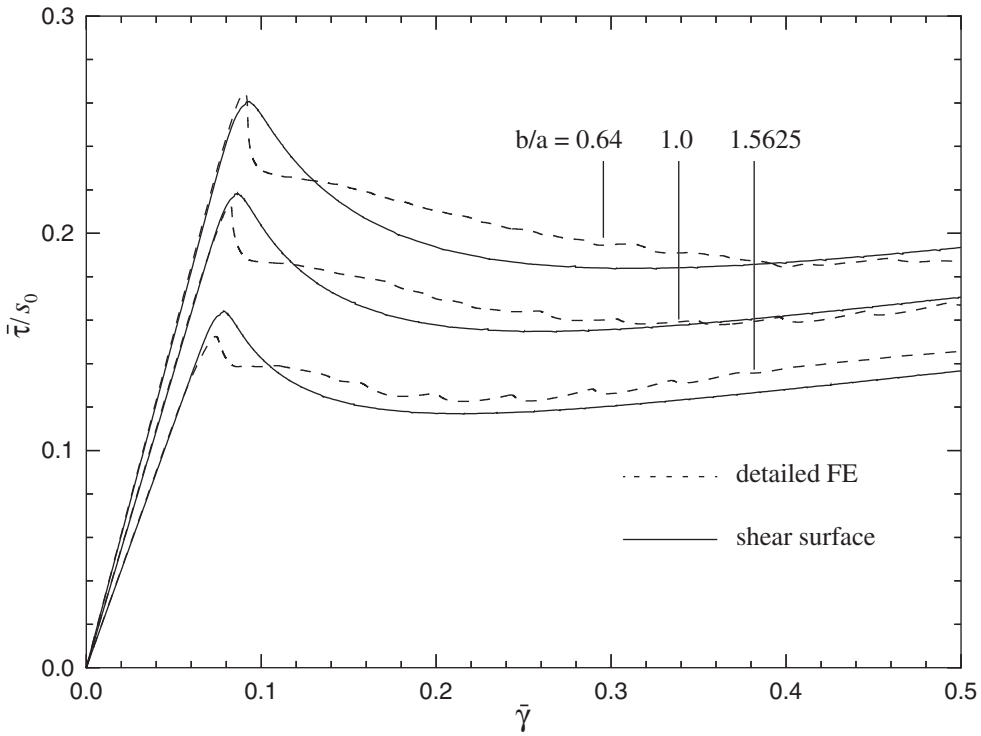

Figure 11. Comparison of stress–strain curves of the shear surface model (Figure 5) with the cell calculations for different aspect ratios of the basic cell, $b/a = 0.64, 1.0$ and 1.5625.

use the configuration of 500 randomly distributed voids shown previously in Figure 3. This configuration is regarded to be repeated in both directions and periodic boundary conditions are applied. The system is subjected to overall simple shear. Since the microstructure now changes from a regular stacking to a random distribution of voids and the applied loading is therefore no longer aligned with the ordering in the microstructure (see also discussion in Section 3.1), we can no longer use the elastic constants as determined by the cell calculations. Instead we use values for Young's modulus and Poisson's ratio that apply to a random stacking of aligned hollow cylinders in a matrix material. In this case, the elastic constants of the voided material are related to those of the matrix (denoted by subscript m) according to [17, 18].

$$E = \frac{(1-f)E_{\mathrm{m}}}{1+f(2-3v_{\mathrm{m}}^2)}, \quad v = \frac{(1-f)v_{\mathrm{m}} + f(1-2v_{\mathrm{m}}^2)}{1+f(2-3v_{\mathrm{m}}^2)} \tag{11}$$

Figure 12 shows the shear bands in the random microstructure at the overall yield point. We see that although the microstructure is not aligned with the direction of applied shear, a 'macroscopic' shear band in this direction is formed by the linking-up of many individual shear bands. As the applied shear was gradually increased, a few shear surfaces were activated, and due to the resulting internal stress redistribution neighbouring ones became active, thus

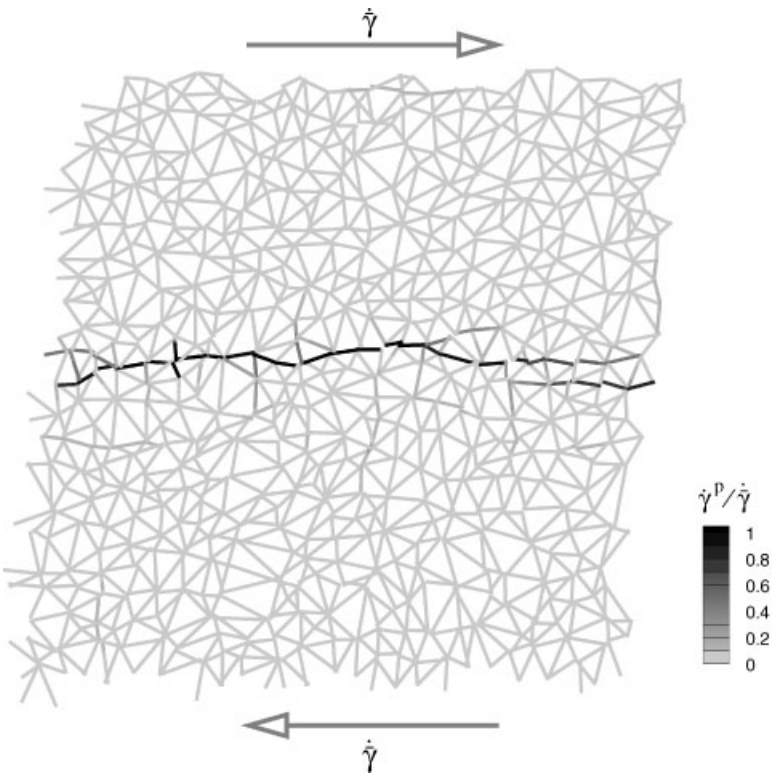

Figure 12. Distribution of plastic shear rate $\dot{\gamma}^p$ in the shear surfaces of a blend containing 500 particles (as in Figure 3) at the moment of yield. The applied loading is simple shear in the horizontal direction.

leading to the situation shown. Despite the coarse representation in terms of shear surfaces, a horizontal path appeared in the material that enables it to accommodate the applied shear. Qualitatively, this is what one would expect.

Figure 13 shows the stress–strain curve corresponding to the calculation of Figure 12. We notice that the sharp yield peak that is seen in the homogeneous matrix (inset of Figure 1) and in calculations with regular arrays of voids, e.g. Figure 11, is reduced. This effect of a randomized microstructure has been found by others as well (see, e.g., Reference [9]).

5. DISCUSSION AND OUTLOOK

The distributed shear surface model presented in this paper is designed to describe the shear banding in a 2D blend containing many particles (or voids once the particles have cavitated). Its resolution is in between a detailed finite element representation around individual voids and a truly homogenized model. An important distinction with the latter is that the present model does not only depend on the volume fraction of rubber particles or voids but also on their spatial distribution. Different such microstructures with the same particle/void volume

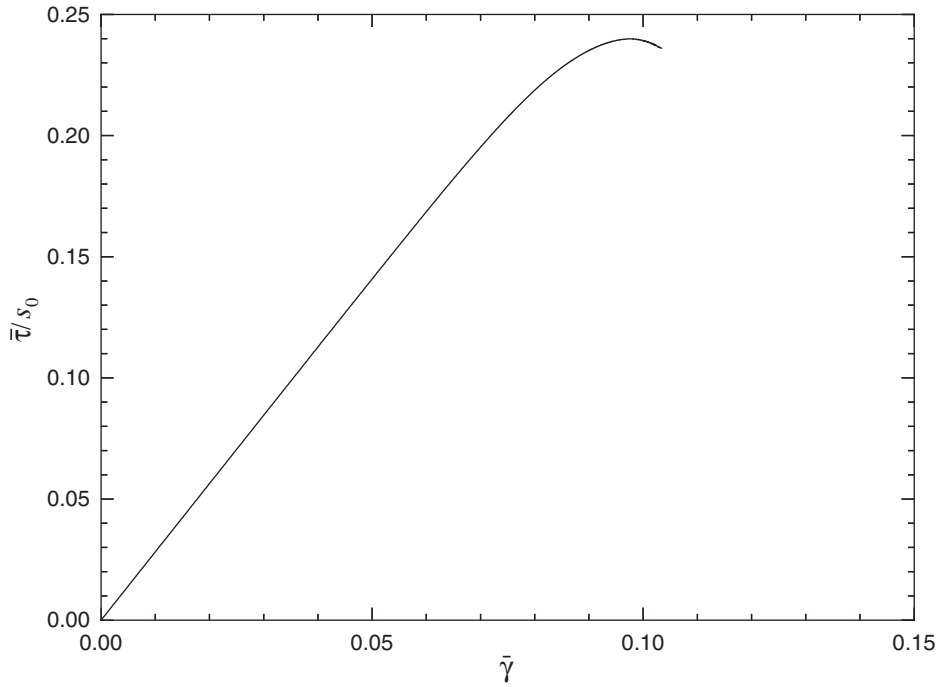

Figure 13. Overall stress–strain curve corresponding to Figure 12.

fraction are represented differently. Moreover, blends with the same particle/void volume fraction, but with another particle/void size will not have the same microstructure and will be represented differently.

The shear surface constitutive law needs to be tuned to the behaviour of the matrix material under consideration (here SAN). For this purpose one needs to consider a number of model micro-level calculations as discussed in Section 3.1 in order to obtain the constitutive parameters. A number of them are identical to the ones used in the micro-level constitutive model, others need to be obtained as a scale-transition from the micro-level calculations. The way to do the latter is not unique; we have described one way that yields reasonable agreement with micro-level computations in terms of the overall stress–strain characteristics and yield conditions under different stress states.

The specific microstructure used for the validation here has been specifically designed to allow for large deformations in the shear surfaces in the direction of applied shear. In this way all the important characteristics of the material response could be investigated. In a random microstructure, as for example in the previous section, such large deformations may not be reached, because of constraints due to the surrounding material.

By its nature, a single shear surface is not very well suited to respond to deformation modes with a high hydrostatic component, because it will only allow deformation parallel to it. This does not have to represent a big problem as long as the region of high hydrostatic stress contains several shear surfaces. In this case it will be possible to activate several shear surfaces that together can accommodate the applied deformation.

The formulation of the shear surfaces so far has presumed voids of equal size, so that the void radius is uniquely determined by the volume (or area) fraction f through

$$N\pi r_{\mathrm{v}}^2 = fS \Rightarrow r_{\mathrm{v}} = \sqrt{\frac{fA}{N\pi}} \tag{12}$$

where N is the number of particles in the region with area S. In a real blend, however, the voids will have a certain size distribution. This can be accounted for quite easily. It should be noted that the critical parameter is the ligament length l in between voids. For a uniform void size, this length is given by

$$l_{\mathrm{u}} = |\mathbf{R}_1 - \mathbf{R}_2| - r_1 - r_2 = |\mathbf{R}_1 - \mathbf{R}_2| - 2r_{\mathrm{v}} \tag{13}$$

($\mathbf{R}_i$ is the position vector of the void and r_i its radius), while for random void sizes it is given by

$$l_{\mathrm{r}} = |\mathbf{R}_1 - \mathbf{R}_2| - (r_1 + r_2) \tag{14}$$

For a given configuration of void sizes and locations the ligament lengths are known and can be used in the integration over the shear surface (see Section 2.3).

Another way of looking at random void sizes is as follows. Since essentially all we prescribe in the model used so far is the position of the voids and the ligament length, we cannot distinguish cases for which $r_1 + r_2 = 2r_{\mathrm{v}}$. Of course, it is not possible to fulfill this condition on all three sides of any given triangular bulk element at the same time. But to a first approximation one might argue that cases with uniform void size or with random void size would be comparable as long as

$$\sum_{i=1}^{N} r_i = Nr_{\mathrm{v}} \tag{15}$$

However, the void volume fraction (in 2D) scales with r^2, not with r, cf. (12). But then, (15) implies

$$\sum_{i=1}^{N} r_i^2 \leqslant Nr_{\mathrm{v}}^2 \Rightarrow f_{\mathrm{r}} \leqslant f_{\mathrm{u}} \tag{16}$$

from which we see that random void sizes correspond to a lower volume fraction f_{r}. This means that with a single mesh, it is possible to compare different statistical distributions of void sizes. The provision, of course, is that for each calculation we use the corresponding volume fraction, following from

$$f = \frac{1}{A}\sum_{i=1}^{N} \pi r_i^2 \tag{17}$$

with A the area of the sample, in determining the elastic constants from Equations (11).

The example in the previous section has shown that the shear surface model is a computationally efficient tool for studying regions or samples of blends containing large numbers of voids. Standard finite element approaches with a detailed resolution of all the shear bands become practically prohibited when there are more than a few voids. An example where the shear surface approach may prove its power is the numerical study of the deformation

fields around a crack in a blend, where the plastic zone contains large numbers of particles. A limiting factor in this application may be that the present approach is based on a given void distribution which is fixed, whereas large plastic flow may lead to substantial void growth [4]. The importance of this will be investigated in a subsequent paper.

REFERENCES

1. Pearson RA, Sue H-J, Yee AF. *Toughening of Plastics*. ACS Symposium Series 759. Oxford University Press: Oxford, 2000.
2. Donald AM, Kramer EJ. Plastic deformation mechanisms in poly(acrylonitrile-butadiene-styrene) [ABS]. *Journal of Materials Science* 1982; **17**:1765–1772.
3. Boyce MC, Parks DM, Argon AS. Large inelastic deformation of glassy polymers, Part I: rate dependent constitutive model. *Mechanics of Materials* 1988; **7**(1):15–33.
4. Steenbrink AC, Van der Giessen E, Wu PD. Void growth in glassy polymers. *Journal of the Mechanics and Physics of Solids* 1997; **45**(3):405–437.
5. Steenbrink AC, Van der Giessen E. On cavitation, post-cavitation and yield in amorphous polymer-rubber blends. *Journal of the Mechanics and Physics of Solids* 1999; **47**(4):843–876.
6. Pijnenburg KGW, Steenbrink AC, Van der Giessen E. Shearing of particles during crack growth in polymer blends. *Polymer* 1999; **40**(21):5761–5771.
7. Pijnenburg KGW, Van der Giessen E. Mesoscopic localized deformations in rubber-toughened blends. In *Toughening of Plastics* Pearson RA, Sue H-J, Yee AF (eds). ACS Symposium Series 759. Oxford University Press: Oxford, 2000; 36–49.
8. Socrate S, Boyce MC. Micromechanics of toughened polycarbonate. *Journal of the Mechanics and Physics of Solids* 2000; **48**(2):233–273.
9. Smit RJM, Brekelmans WAM, Meijer HEH. Prediction of the large-strain mechanical response of heterogeneous polymer systems: local and global deformation behaviour of a representative volume element of voided polycarbonate. *Journal of the Mechanics and Physics of Solids* 1999; **47**(2):201–221.
10. Lazzeri A, Bucknall CB. Applications of a dilatational yielding model to rubber-toughened polymers. *Polymer* 1995; **36**(15):2895–2902.
11. Pijnenburg KGW, Van der Giessen E. Macroscopic yield in cavitated polymer blends. *International Journal of Solids and Structures* 2001; **38**(20):3575–3598.
12. Xu X-P, Needleman A. Numerical simulations of fast crack growth in brittle solids. *Journal of the Mechanics and Physics of Solids* 1994; **42**(9):1397–1434.
13. Tijssens MGA, Sluijs LJ, Van der Giessen E. Numerical simulation of quasi-brittle fracture using damaging cohesive surfaces. *European Journal of Mechanics – A/Solids* 2000; **19**(5):761–779.
14. Argon AS. A theory for the low-temperature plastic deformation of glassy polymers. *Philosophical Magazine* 1973; **28**:839–865.
15. Wu PD, Van der Giessen E. On improved network models for rubber elasticity and their applications to orientation hardening in glassy polymers. *Journal of the Mechanics and Physics of Solids* 1993; **41**(3): 427–456.
16. Wu PD, Van der Giessen E. Computational aspects of localized deformations in amorphous glassy polymers. *European Journal of Mechanics – A/Solids* 1996; **15**(5):799–823.
17. Zhao YH, Tandon GP, Weng GJ. Elastic moduli for a class of porous materials. *Acta Mechanica* 1989; **76**(1/2):105–131.
18. Christensen MR. *Mechanics of Composite Materials*. Wiley: New York, 1979.

